Water Uptake of Tape-Cast Cathodes for Lithium Ion Batteries

U. Langklotz[1], M. Schneider[*2], A. Michaelis[1, 2]

[1]TU Dresden, Institut für Werkstoffwissenschaft (Institute of Material
Science), Helmholtzstr. 7, 01069 Dresden, Germany
[2]Fraunhofer IKTS Dresden, Winterbergstr. 28, 01277 Dresden, Germany

Abstract

High-performance ceramic-based cathodes (e.g. NMC, LFP) are the backbone of lithium ion batteries. The production of cathodes is based on ceramic manufacturing technologies (powder processing, slurry, tape casting). The minimization of the water content in the fabricated battery is a crucial point in its manufacturing.

This work is focused on the kinetics of water uptake in tape-cast cathode materials (NMC, LFP). The cathode foils were exposed to atmospheres with varying humidity and the water content was determined by means of coulometric Karl-Fischer titration. Conversely, the tendency of the cathodes to release residual water is examined.

Additionally, electrochemical investigations were performed on cathode foils containing defined amounts of water. Galvanostatic charge-discharge experiments were conducted in 2-electrode Swagelok® cells versus graphite anodes. It could be shown that the influence of residual water on the cell performance is very complex. On the one hand, the residual water causes side reactions. On the other hand, low water content obviously supports the formation of the solid electrolyte interface (SEI) on the anode.

Keywords: Lithium ion battery, residual water, LFP, NMC, solid electrolyte interface

I. Introduction

A wide variety of cathode materials for lithium ion batteries are currently under investigation. Lithium nickel manganese cobalt oxide (NMC), $Li(Ni_{0.33}Mn_{0.33}Co_{0.33})O_2$ and lithium iron phosphate (LFP), $LiFePO_4$ are representative materials [1]. As anode materials, generally various carbonaceous species, such as graphite, are used [2,3].

Nevertheless, all the various methods of synthesis and processing of active material and complete electrode foils are based on ceramic technologies. In cathode processing, for example, the active material is mixed with a polymer binder and a conductive agent. The slurry is tape-cast onto an aluminium foil as a current collector.

Owing to the fact that several components of the lithium ion battery, particularly the electrolyte, are very sensitive to humidity, low water content is necessary. The water reacts with the conductive lithium salts of the electrolyte, e.g. $LiPF_6$, and forms acidic species such as HF [4,5].

$$LiPF_6 + H_2O \rightarrow 2HF + LiF + POF_3 \qquad (1)$$
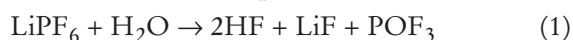
This reaction leads to various problems within the battery cell. For example, the loss of conductive salt decreases the electrolyte conductivity, which contributes to an increase in cell resistance, and diminishes cell capacity [6]. Reaction products such as HF can cause the active material to decompose as reported explicitly for $LiMn_2O_4$ [7,8].

Furthermore, water can be electrochemically decomposed at the anode at potentials below $1.5\ V_{Li/Li}+$ [9]. Thus

water is also involved in the formation of surface electrolyte interface (SEI) films that usually develop by means of electrolyte decomposition at the anode. Besides the organic components of the electrolyte, water traces and their reaction products can strongly influence the composition and properties of the growing SEI [10, 11, 12].

It is well known that protic impurities such as water severely impair battery cell performance [13, 14]. Therefore a crucial point is the minimization of the water content within the battery during processing. The processing of lithium ion batteries is generally conducted in a dry atmosphere. Furthermore, the electrode foils are dried during assembly. This fact correlates to the work of Saharan *et al.*, who postulate that the cathode materials can be a main source of water within the cell [15]. Surprisingly, no information is available concerning the water uptake mechanism of tape-cast cathode foils in literature. Therefore this work presents a systematic investigation on the water content of tape-cast cathode foils based on LFP and NMC as active materials. The mechanisms of water uptake and release are examined with respect to treatment conditions that are close to industrial processing. Moreover, the influence of the residual humidity of the cathode foil on the performance of the whole battery cell is investigated.

II. Experimental

The investigations of the water content were conducted on two different tape-cast cathode foils. They are briefly described in Table 1.

* Corresponding author: michael.schneider@ikts.fraunhofer.de

Table 1: Specifications of the two different tape-cast cathode foils investigated in this work.

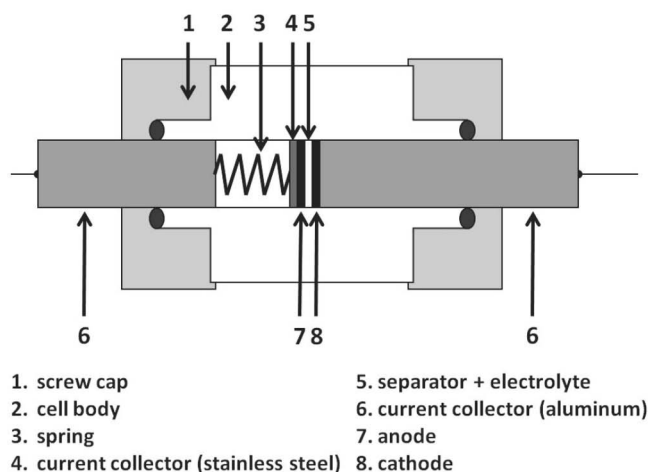| Active material	LFP (P2, *Südchemie*), 90 mass%, LiFePO$_4$ (carbon coated)	NMC (in-house product), 96 mass% Li(Mn$_{0.37}$Co$_{0.35}$Ni$_{0.35}$)O$_{2.07}$
Particle size d$_{50}$	0.8 μm	2.0 μm
Binder	polyvinylidene-difluoride (PVDF) Type 5130 (*Solvay*), 6 mass%	polyvinylidene-difluoride (PVDF) Type 5130 (*Solvay*), 2 mass%
Conducting agent	carbon black SuperP-Li (*Timcal*), 4 mass%	carbon black SuperP-Li (*Timcal*), 2 mass%
Current collector	aluminium foil, 40 μm thickness	
Thickness	45 – 50 μm	71 – 85 μm
Mass coverage	10 mg/cm²	21 – 25 mg/cm²
BET surface area	9.8 m²/g	2.7 m²/g
Gravimetric capacity (measured CC/CV with 0.2C)	125 mAh/g	130 mAh/g

For investigation of water uptake, the cathode foils are exposed to atmospheres with different humidity for 1 hour, 1 day and 1 week. A relative humidity (rh) of 15 %, 40 % and about 90 % was realized with glycol-water mixtures and controlled with a hygrometer. Additionally, samples were stored in an argon-filled glove box for several weeks and investigated as a reference.

For drying experiments, the water content of the foils was adjusted to a certain value by exposing the samples to an atmosphere with 15 % humidity for one hour. Afterwards the moisturized samples were dried under varying parameters:

1. Samples were stored in an argon-filled glove box (< 1 ppm water) over 2 days and 5 weeks
2. Samples were dried in a vacuum compartment dryer attached to the glove box
   - T = 100 °C, 120 °C, 200 °C over 15 h
   - T = 120 °C over 3, 15 and 72 h
   - T = 120 °C over 15 h, with variation of the initial water content of the samples

The water content was determined by means of coulometric Karl-Fischer titration (KFT) at a heating temperature of 200 °C. The water content is given in ppm by weight in all cases. The applied device was a C30 compact Karl Fischer coulometer coupled with a Stromboli KF oven sample changer (*Mettler Toledo*). The heating temperature of the oven was 200 °C. The reagent for the titration cell was Hydranal®-Coulomat AD (*Sigma-Aldrich*). The weighed portion was in the range of 0.8 to 1.2 g and was exactly determined before experiment starts.

For electrochemical investigations, 2-electrode Swagelok® cells as schematically shown in Fig. 1 are used. The water content of the cathodes was set to certain values by exposing them to 15 %, 40 % and 90 % humidity for one hour. Additionally, samples that were stored in the glove box for 5 weeks and samples that were dried at 120 °C were investigated. Commercially available graphite-based anode foils (3mAh/cm²/320mAh/g, *MTI*) were used as anode. It was stored in the glove box for several weeks and

1. screw cap
2. cell body
3. spring
4. current collector (stainless steel)
5. separator + electrolyte
6. current collector (aluminum)
7. anode
8. cathode

Fig. 1: Schematic drawing of the 2-electrode Swagelok® cell setup used for electrochemical investigations.

its water content amounted to about 90 ppm (determined by means of KFT). The electrolyte was LP40 (1M LiPF$_6$ in EC:DEC (1:1 wt), *Merck*), containing less than 20 ppm water. A polyethylene-nonwoven (Viledon®, *Freudenberg*) was used as a separator. The cells were completely assembled in an argon-filled glove box.

Current-controlled charge-discharge cycles were performed with a multichannel galvanostat/potentiostat (VMP3, *Biologic*). The experimental conditions are listed in Table 2.

Table 2: Conditions for the galvanostatic charge-discharge experiments.

Cathode	LFP foil	NMC foil
Charge rate	C/6.5	C/6.5
Current density /mA/cm²	0.2	0.4
U$_{limit}$/V	2.5...3.7	3.0... 4.2
Number of cycles	30	30

III. Results

(1) *Water uptake of cathode materials*

An overview of the water content of the cathode foils is given in Fig. 2a. The different symbols represent different exposition times. The symbols deviate slightly around the intended humidity, representing the real humidity value measured with a hygrometer. Generally, the LFP-based cathode foil contains approximately 2.5 times more water than the NMC cathode foil. Obviously the influence of the exposition time is small, while the air humidity plays a key role for the water content of the samples. Indeed, the shape of the curve resembles the course of adsorption isotherms according to Brunauer, Emmett and Teller (BET) [16, 17].
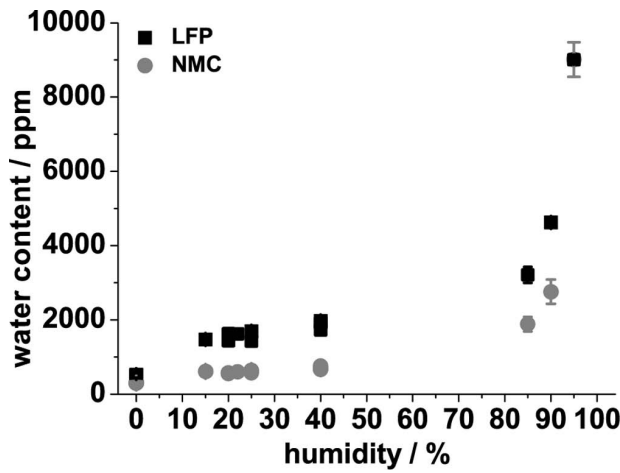
Fig. 2a: Water content of the electrodes in dependence on the atmospheric humidity.

The BET model describes the adsorption of molecules from the gas phase at a solid substrate (adsorbent). The observed correlation between the adsorbed molecules and their concentration in the gas phase follows Eq. (2):

$$V = \frac{V_{mono}cp}{p_0(1-\frac{p}{p_0})(1-\frac{p}{p_0}+C\frac{p}{p_0})} \qquad (2)$$

where V is the volume of the adsorbate, V_{mono} the volume of one monolayer of the adsorbate, c the BET constant, p the equilibrium vapour pressure and p_0 the saturated vapour pressure in the gas phase. The measured water content and air humidity correlate to the volume of adsorbate, V, and the equilibrium vapour pressure, p. According to the theory, the water uptake can be divided into three ranges (see Fig. 2b):

1. low humidity (< 10 %) – range of partial covering of the surface
2. moderate humidity (10 – approx. 70 %) – formation of a monolayer of adsorbate on the adsorbent
3. high humidity (> 70 %) – formation of water multilayer on the surface

However, there are distinct differences in the amount of water adsorbed by the cathode foils. In the range of monolayer formation the LFP-based foil showed approximately a 2.5-times-higher water content in comparison with the NMC sample. The amount of adsorbed water depends on the heat of adsorption of water as well as on the accessible surface of the electrode foil.
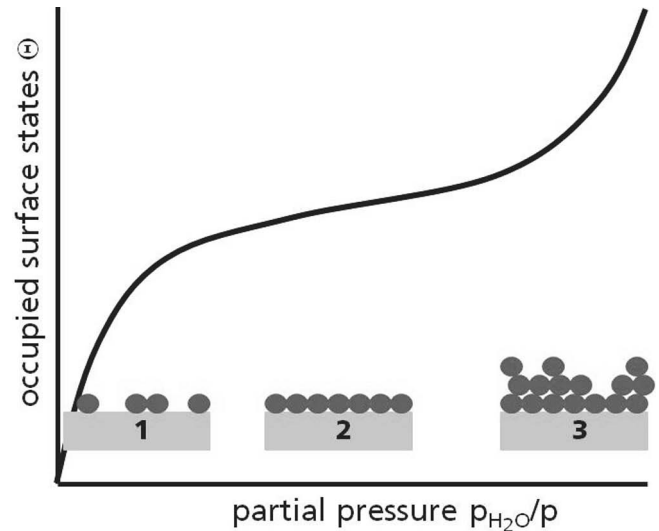
Fig. 2 b: Theoretical course of a BET-isotherm and schematically drawn surface states.

BET measurements result in surface areas of approximately 9.8 m²/g for the LFP foil and 2.7 m²/g for the NMC foil. Consequently, the ratio between the surface areas of both materials is 3.6 : 1 (LFP : NMC). This value is significantly higher than the ratio of the water contents of 2.5 : 1. Assuming comparable radii of the adsorbed water on the surface of LFP and NMC, similar heats of adsorption and equal air humidity, Eq. (2) can be transformed into:

$$\left(\frac{V}{V_{mono}}\right)_{LFP} = \left(\frac{V}{V_{mono}}\right)_{NMC} \qquad (3)$$

The water content in the range of monomolecular covering equals the volume of one monolayer. As a consequence the relation of water contents should be the same as the relation of the surface areas. However, both values deviate, which indicates different heats of adsorption for the active materials. According to our results, it is smaller for LFP in comparison to NMC.

Indeed, the matrix of conductive carbon and PVDF binder does not significantly affect the adsorption behaviour. This was proven by additional investigations of the pure active material powders not shown here, which were highly incident to the results for the tape-cast cathode foils.
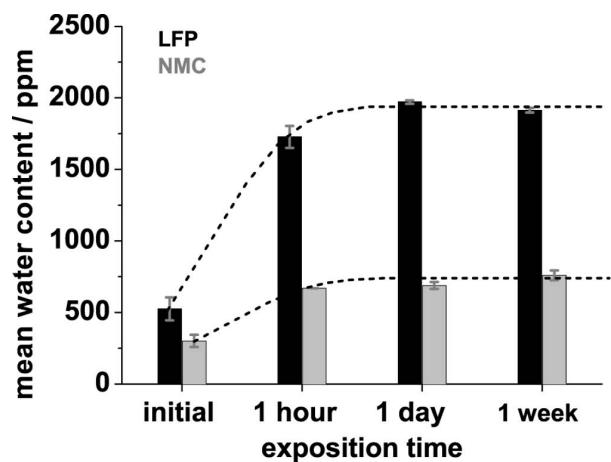
Fig. 3: Water uptake of the electrodes in dependence on the time of exposition in an atmosphere with a defined relative humidity of 40 %. The broken lines illustrate the development of water uptake over the time in principle.

The time dependence of water uptake is shown in Fig. 3. The water content increases rapidly and reaches a steady state after about one hour of exposure for both materials. The steady-state water content of the sample is defined by the air humidity according to Fig. 2a. The time dependence of the water uptake can be described by Eq. (4):

$$\frac{dc_{ads}}{dt} = r_{ads} = k_{ads}(1-\Theta)p_i \tag{4}$$

Therein the adsorption rate, r_{ads}, is defined as the increase in the concentration of adsorbed molecules, c_{ads}, per time t. It depends on the rate constant k_{ads}, the number of adsorbed molecules Θ and the equilibrium vapour pressure, p_i. The bigger k_{ads}, the faster the adsorption, and the earlier the steady-state value of water content is achieved.

(2)   *Water release of cathode materials*

Based on the results described in section III (1), the water release during drying is examined in the following. Fig. 4 shows the water content of humidified samples after storage in the glove box for certain durations. The water con-
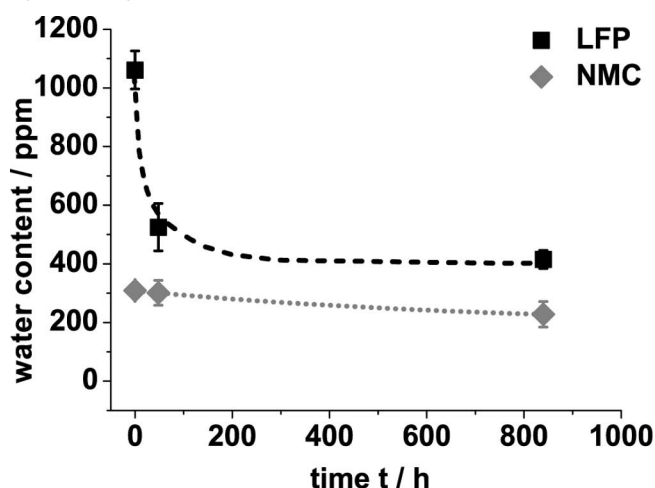

Fig. 4: Water release of the electrodes in dependence on the time of exposition in a dry atmosphere (relative humidity < 1 ppm).

tent in the glove box atmosphere is approximately 1 ppm. The humidified samples release water in such a dry atmosphere in accordance with Eq. (5):

$$-\frac{dc_{ads}}{dt} = r_{des} = k_{des}\Theta \tag{5}$$

The rate of desorption, r_{des}, depends on the number of adsorbed molecules Θ and the rate constant k_{des}. The rate constant of desorption, k_{des}, is the reciprocal value of k_{ads}. If k_{ads} is very high, then k_{des} must be very low. Therefore, the steady-state value of water content is only reached after about 250–300 h for the desorption (Fig. 4). The overall progress can be described by the time law for a reaction of first order (Eq. (6)):

$$-\ln c_{ads} = k_{-1}t \tag{6}$$

The final water content, after five weeks storage in a water-free atmosphere, amounts to about 100 ppm in NMC foil and 300 ppm in LFP foil. Again, this difference is caused by the different surface areas and heats of adsorption of the two materials. Owing to the fact that formulas (5) and (6) only describe the rate of equilibration, it can be stated that an increase in the drying time cannot further

improve the achieved water content. The final water content is defined by the steady state according to Eq. (2).

However, the water content of the tape-cast foils is influenced by the temperature during drying (see Fig. 5a and b). The drying temperature interacts in two different ways.
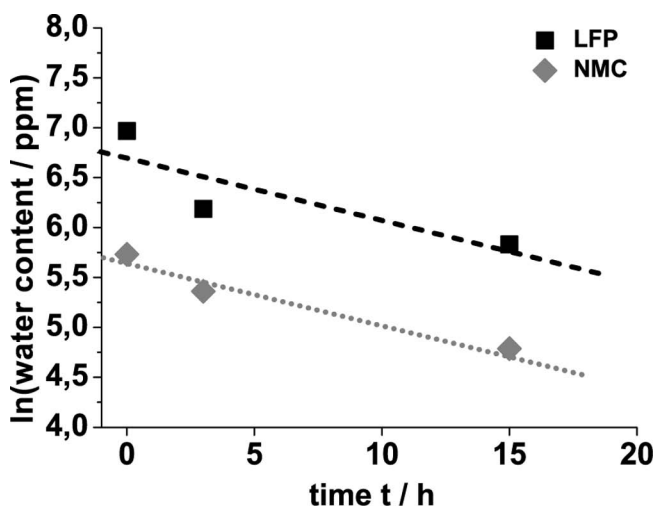

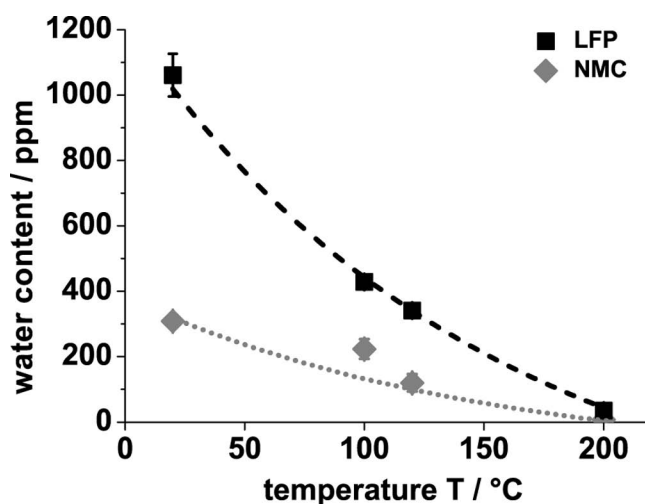**Fig. 5 a:** Drying at 120 °C for varying time.

Fig. 5 b: Drying for 15 h at 100 °C, 120 °C and 200 °C.

In the first instance, the rate constants depend on the temperature as described by the Arrhenius equation (Eq. (7)). This implies faster equilibration with increasing temperature, as the rate constant of desorption exponentially increases:

$$k_{des} = A \exp\left\{-\frac{E_A}{kT}\right\} \tag{7}$$

Fig. 5a shows the water content of samples dried in vacuum at 120 °C for several durations. Now the steady state is reached already after about 15 h owing to the increased rate constant of desorption.

Additionally, the temperature influences the emerging equilibrium. This correlation is shown in Fig. 5b. Here the drying of the samples is performed at various temperatures for 15 h. With respect to Fig. 5a, equilibration can be assumed after that time. Obviously, the water content of the samples decreases with increasing drying temperature. The steady state of water content shows a complex dependence on the water concentrations in the adsorbent and in

the gas phase as well as on the temperature. This correlation can be described by an isobar according to H. Freundlich [18] (Eq. (8)):

$$q + RT = RT^2 \left(\frac{d \lg p}{dT} \right)_\Theta \tag{8}$$

with the molar differential heat of adsorption q, the temperature T, the gas constant R and the temperature coefficient of the logarithm of the equilibrium vapour pressure under isosteric conditions, $(d \lg p/dT)_\Theta$. In this case a drying temperature of 200 °C gave the best results. Nevertheless, for practical application the drying temperature is limited by the thermal stabilities of the electrode. Especially the PVDF binder is known to undergo crystallization above 150 °C [19,20]. Therefore the drying temperature should not exceed 120 °C to avoid such structural changes, although this results in a slightly higher water content within the electrodes.

Usually, the electrode drying procedure is conducted under reduced pressure. However, the influence of the reduced pressure is rather complex and difficult to describe. On the one hand, the technical vacuum conditions realized in the compartment dryer used represent an almost water-free atmosphere, similar to the conditions in the glove box. Thus they affect the steady-state water content. On the other hand, the reduced pressure is an additional driving force influencing the rate of equilibration. However, the influence of vacuum on the drying procedure was not a focus of our current investigations.
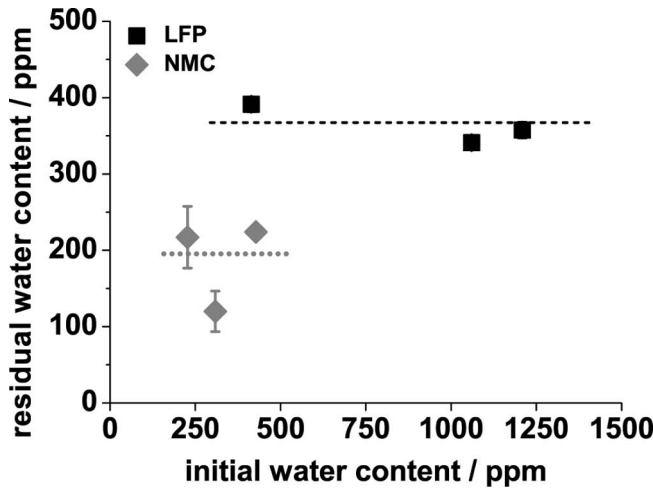

Fig. 6: Water content after drying in dependence on the initial water content.

According to the discussion above, it can be postulated that the drying procedure is also based on an equilibration process. The achievable water content in the electrodes is a steady-state value, depending on the properties of the active material (surface area, heat of adsorption), on the temperature, the atmospheric humidity and the pressure. The water content always equilibrates to a certain steady state providing the drying time is long enough. Consequently, the residual water content after drying under certain conditions is independent of the initial state of the samples. This is clearly shown in Fig. 6. The water content after drying (120 °C, vacuum, 15 h) is plotted as a function of the initial water content. Corresponding to the theory, the re-

sulting humidity does not depend on the initial state, neither for NMC nor for LFP.

(3) *Influence of water content on the electrochemical performance*

The cathodes for lithium ion batteries always contain a certain amount of water, as it could be shown in section III (2). Therefore, it is necessary to clarify the influence of the water on the electrochemical performance of lithium ion cells. The materials used, NMC and LFP as cathodes and graphite as anode, as well as the chosen cell setup are close to commercial battery systems (see Fig. 1). The impact of humidity on the charge-discharge behaviour is examined.
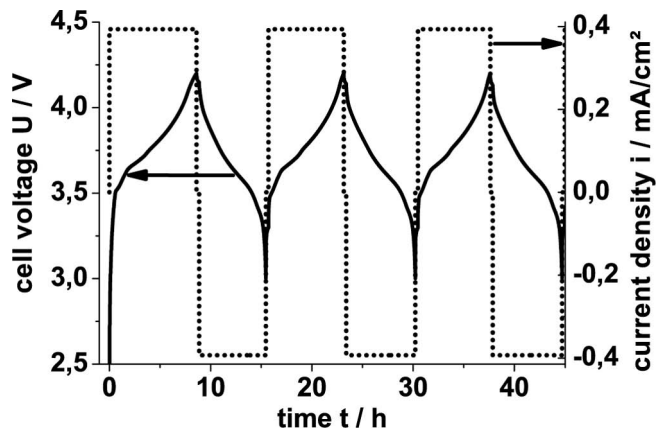

Fig. 7 a: Charge-discharge cycles of a cell consisting of an NMC cathode and carbon-anode.
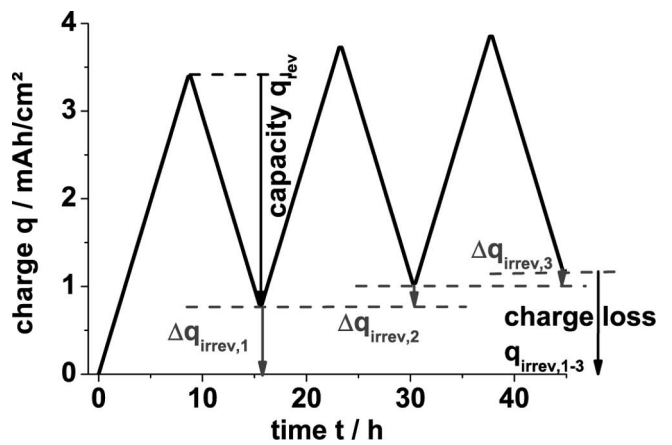

Fig. 7 b: Charge flow during the cell cycling shown in Fig. 7 a.

Fig. 7a shows the current-voltage relation over the cycling procedure. The charge quantity which is converted during the charge-discharge cycles and calculated from Fig. 7a is shown in Fig. 7b. The charge quantity can be divided into two parts:

$$q = q_{rev} + q_{irrev} \tag{9}$$

1. The charge q_{rev} flows into the (reversible) delithiation/lithiation reactions at the electrodes. This charge can be regained during discharging and is equal to the capacity of the cell.

2. The charge q_{irrev} flows into (irreversible) side reactions (e.g. electrolyte decomposition, SEI formation, electrolysis of water) and is accumulated over the total number

of cycles. This part can be separated for every charging cycle, resulting in the single charge losses $\Delta q_{irrev,1}$, $\Delta q_{irrev,2}$ ... $\Delta q_{irrev,n}$:

$$q_{irrev,1-n} = \sum_{i=1}^{n} \Delta q_{irrev,i} \qquad (10)$$

Based on the literature [6, 21], the authors use the capacity fading as a measure for the cycling performance of the cell.

The residual water within a lithium ion cell strongly affects the electrolyte decomposition and SEI formation and its properties (see e.g. [11, 12]). On one hand, decomposition products such as hydrofluoric acid harm the cathodes, e.g. by leaching of manganese (in NMC) and iron ions (in LFP) [7, 8, 22]. This mechanism decreases the cell capacity. On the other hand, mobile lithium is trapped within the SEI, also leading to capacity fading [6]. The correlation between SEI formation and properties and the cell capacity is rather complex. Therefore, the authors intend to evaluate the intensity of electrochemical side reactions by measuring the capacity fading as well as the charge loss as indicators of the influence of water on the cell performance.
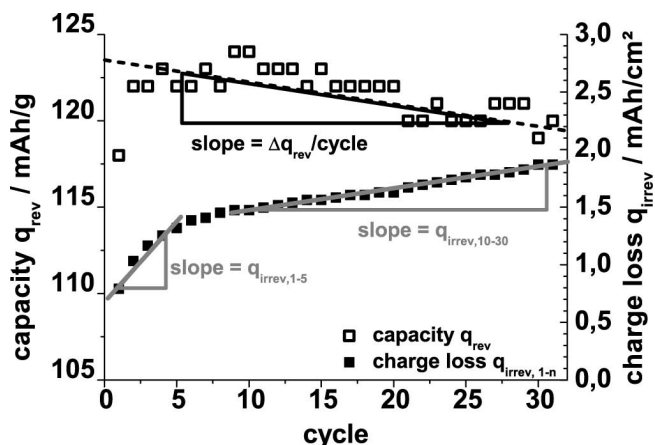

Fig. 8: Determination of the capacity loss Δq_{rev}/cycle and the charge loss $q_{irrev,1-n}$ from the experimental data, for the example of an NMC graphite cell.

The capacity loss per cycle, Δq_{rev}/cycle, is determined from the slope of the capacity over cycle plot (Fig. 8). Owing to the fact that both cathode foils are dimensioned for different capacities, the relative capacity loss $\Delta q_{rev,rel}$ is calculated to enable the comparison of both materials:

$$\Delta q_{rev,rel} = \frac{\Delta q_{rev}}{cycle} \cdot \frac{1}{q_{rev,1}} \qquad (11)$$

where $q_{rev,1}$ is the reversible capacity of the first discharging. The specific capacities amount to $q_{rev,1} = 2.7$ mAh/cm² for NMC and $q_{rev,1} = 1.2$ mAh/cm² for LFP, which is equivalent to gravimetric capacities of about 120 mAh/g for both materials. These results match well with the gravimetric capacities of the cathode materials given in Table 1.

The charge loss per cycle, $q_{irrev,1-n}$, is analogically determined from the slope of certain ranges of the q_{irrev} over cycle plots (Fig. 8). These values are not referred to the value from the first cycle, as the side reactions depend on the electrode surface more than on its capacity.

Generally, the capacity fading can be caused by an increase in cell impedance and/or by materials degradation and loss of active electrode material respectively. Howev-

er, the evaluation of the IR-drops of current-controlled charge-discharge curves shows no influence of the water content. Therefore, the authors interpret the capacity fading as a consequence of the degradation of active materials. Traces of water can lead to HF formation according to Eq. (1). As aforementioned hydrofluoric acid is known to leach out components from the active cathode material [7, 8, 22], which decreases the capacity. This mechanism should be strongly related to the content of water and correspondingly the concentration of hydrofluoric acid in the cell. Fig. 9 shows that the capacity loss decreases with increasing amount of water in a range of water content < 2000 ppm. This is a priori in contrast to the assumption that the higher the content of water the stronger the capacity fading. Otherwise, the relative capacity loss of the NMC cell is smaller than for cells with LFP cathodes. At very high water content (≈ 10000 ppm), the LFP-based cell shows severe capacity fading. In contrast, the capacity loss of NMC-based cells remains at a constant low level even with some thousands ppm of water. Based on this observation, the authors assume that LFP cathodes – in contrast to NMC cathodes – are highly sensitive towards high water contents. At this point, it should be noted that LFP particles are coated by carbon. Holze *et al.* reported that graphite anodes are highly sensitive towards humidity of > 1000 ppm [23, 24]. Though the reaction mechanisms at the LFP cathode differ from those at a graphite anode, the carbon coating might be affected by the moisture in the cell. This can cause degradation similar to the degradation of graphite anodes as described by Holze *et al.* [23, 24].
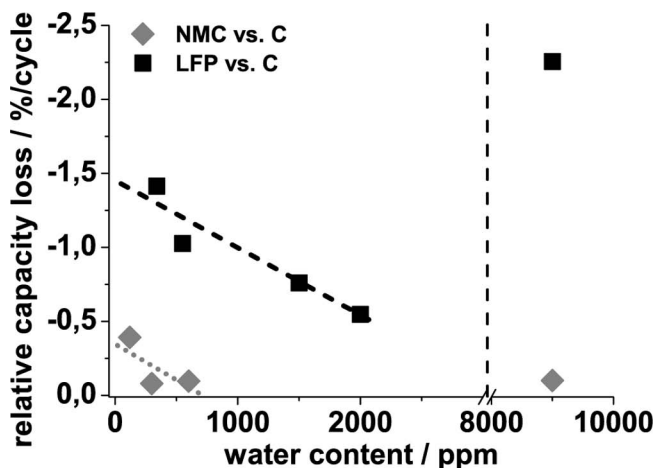

Fig. 9: Relative capacity loss for various cell compositions in dependence on the water content within the cathode.

Besides the discussed mechanism, the SEI strongly influences the cycling stability of a cell. Concerning the SEI formation, water is known to influence the composition and insulating properties of the interphase [11, 12]. The presence of small amounts of water seems to improve the stability of the SEI. However, the interactions between water content, SEI formation and re-dissolution and cathode material degradation are rather complex and cannot be completely understood based on the experiments presented in this work. Further investigations, including detailed analysis of the cell impedance by means of electrochemical impedance spectroscopy and charge-discharge cycling in a three-electrode setup, are essential.
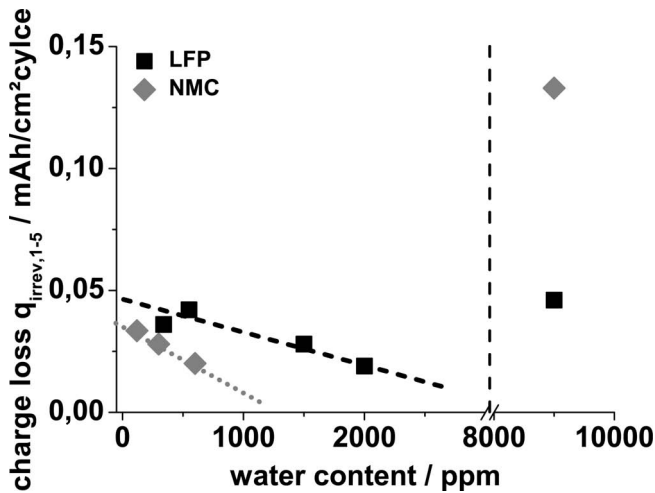
Fig. 10a: Charge loss during the initial five cycles for various cell compositions in dependence on the water content.
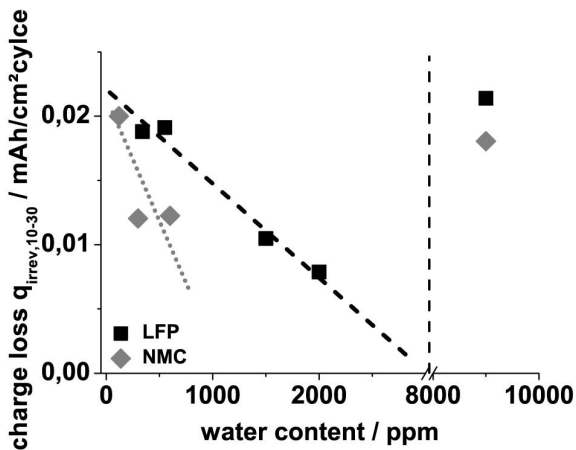

Fig. 10b: Charge loss during the cycles 10 – 30 in dependence on the water content.

The charge loss of the cells is additionally evaluated to aid understanding of the aforementioned observations. The charge loss is attributed to electrochemical side reactions such as decomposition of electrolyte components. The charge losses of the initial five cycles, $q_{irrev,1-5}$, are shown in Fig. 10a as a function of the water content within the cathode. It can be assumed that the SEI formation is completed after this number of cycles [25]. This is in agreement with the data shown in Fig. 8, where the strongest increase of the cumulative charge is limited to the first five cycles.

The behaviour of the charge loss is highly incident to the capacity fading. Again, for low and medium water contents (< 2000 ppm) a decrease of the charge loss can be observed. This can be attributed to SEI formation taking place with higher current efficiency in the presence of water traces. This is presumably due to the contribution of hydroxide species that are formed at the anode below $\varphi = 2\,V$ vs. Li/Li$^+$ [26] (Eq. (12)):

$$H_2O + e^- \rightarrow 0.5\,H_2 + OH^- \qquad (12).$$
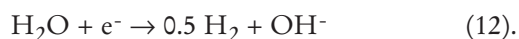
If the cell contains a higher amount of water, the charge loss increases again. According to Holze *et al.* [23,24], this effect can be explained by the degradation of the graphite anode. Graphite exhibits active surface states that tend to react with water, leading to a weakening of the SEI on the anode and a degradation of the graphite structure.

The processes taking place in the early cycles also strongly influence the cell performance during cycles later on. The charge loss of the following charge-discharge cycles, $q_{irrev,10-30}$, is a measure for the properties of the completely formed SEI layer (Fig. 10b). Generally, the charge loss in the advanced state is small in comparison to the initial state of the cycling experiment, owing to better insulating properties of the fully formed SEI. The higher resistance and protective effect of the SEI diminishes the intensity of side-reactions at the anode. Therefore the decrease of charge loss observed for increasing water contents up to < 2000 ppm (Fig. 10b) can be explained based on an improved insulating effect of the SEI when formed in the presence of small amounts of water.

IV. Conclusions

This work was focused on the investigation of the water uptake and release in two different cathode materials for lithium ion batteries. Additionally, basic electrochemical investigations were performed to estimate the influence of the humidity introduced into a battery cell by the cathodes. It could be shown that:

1. The water uptake and release strictly follows the adsorption kinetics according to Brunauer, Emmett and Teller.
2. The water content of an electrode foil is mainly determined by the active surface of the electrode, the atmospheric humidity and the temperature.
3. The kinetic of the water uptake and release is determined by the corresponding rate constants.
4. The influence of water on the electrochemical performance of cells is complex. Main insights are:
   a. Water from the cathode spreads in the whole cell. The trace water influences both anode and cathode.
   b. Small amounts of water seem to improve the formation of SEI layers. This might lead to an increase in SEI formation efficiency, decreased resistances and improved protective behaviour. However, the influence of the water on the SEI and the resulting impact on the cell performance are highly complex and cannot be fully explained based on the current findings.
   c. Very high water contents within the cell cause a deterioration in the cell performance, leading to increase of side reactions and in the case of LFP-cathodes to cell capacity fading. This was ascribed to the known sensitivity of carbonaceous materials (carbon anodes and carbon-coated LFP) towards a high level of humidity.

Preparation, storage and drying procedures can be optimized based on the knowledge of the adsorption kinetics. However, drying procedures always must find a balance between technical effort and attainable water content

References

1   Ohzuku, T., Brodd, R.J.: An overview of positive-electrode materials for advanced lithium-ion batteries, *J. Power Sources*, **174**, 449 – 456, (2007).

2   Kaskhedikar, N.A., Maier, J.: Lithium storage in carbon nanostructures, *Adv. Mater.*, **21**, 2664 – 2680, (2009).

3   Daniel, C., Besenhard, J.O.: Handbook of battery materials. Second, completely revised and enlarged edition, vol.1. Wiley VCH, Weinheim, 2011, 482.

4   Heider, U., Oesten, R., Jungnitz, M.: Challenge in manufacturing electrolyte solutions for lithium and lithium ion batteries quality control and minimizing contamination level, *J. Power Sources*, **81 – 82**, 119, (1999).

5   Barlow, C.G.: Reaction of water with hexafluorophosphates and with li Bis(perfluoroethylsulfonyl)imide salt, *Electrochem. Solid St.*, **2**, 362 – 364, (1999).

6   Abraham, D.P., Knuth, J.L., Dees, D.W., Bloom, I., Christophersen, J.P.: Performance degradation of high-power lithium-ion cells – electrochemistry of harvested electrodes, *J. Power Sources*, **170**, 465 – 475, (2007).

7   Jang, D.H., Shin, Y.J., Oh, S.M.: Dissolution of spinel oxides and capacity losses in 4 V Li/$Li_x Mn_2 O_4$ cells, *J. Electrochem. Soc.*, **143**, 2204 – 2211, (1996).

8   Amatucci, G.G., Pasquier, A.D., Blyr, A., Zheng, T., Tarascon, J.-M.: The elevated temperature performance of the $LiMn_2 O_4$/C system: failure and solutions, *Electrochim. Acta*, **45**, 255 – 271, (1999).

9   Aurbach, D., Talyosef, Y., Markovsky, B., Markevich, E., Zinigrad, E., Asraf, L., Gnanaraj, J.S., Kim, H.-J.: Design of electrolyte solutions for li and Li-ion batteries: a review, *Electrochim. Acta*, **50**, 2/3, 247 – 254, (2004).

10 Lee, H., Cho, J.-J., Kim, J., Kim, H.-J.: Comparison of voltammetric responses over the cathodic region in $LiPF_6$ and Li-BETI with and without HF, *J. Electrochem. Soc.*, **152**, 6, A1193 – A1198, (2005).

11 Joho, F., Rykart, B., Imhof, R., Novak, P., Spahr, M.E., Monnier, A.: Key factors for the cycling stability of graphite intercalation electrodes for lithium-ion batteries, *J. Power Sources*, **81 – 82**, 243 – 247, (1999).

12 Verma, P., Maire, P., Novák, P.: A review of the features and analyses of the solid electrolyte interphase in Li-ion batteries, *Electrochim. Acta*, **55**, 6332 – 6341, (2010).

13 Aurbach, D., Zaban, A., Schechter, A., Ein-Eli, Y., Zinigrad, E., Markowsky, B.: The study of electrolyte solutions based on ethylene and diethyl carbonates for rechargeable li batteries I. li metal anodes, *J. Electrochem. Soc.*, **142**, 2873 – 2882, (1995).

14 Mao, H., Reimers, J.N., Zhong, Q., von Sacken, U., In: Proceedings of the fall meeting of the electrochemical society, Abstract No. 100. Miami Beach, USA, 1994, 159.

15 Saharan, V., Roberts, J., Manev, V., Chia, Y.H., MacLean, G., McCullen, S.R.: Moisture uptake by the positive active material from the casting solvent and the ambient environment, *J. Power Sources*, **146**, 809 – 812, (2005).

16 Brunauer, S., Emmett, P.H., Teller, E.: Adsorption of gases in multimolecular layers, *J. Am. Chem. Soc.*, **60**, 309 – 319, (1938).

17 Langmuir, I.: Adsorption of gases on glass, mica and platinum, *J. Am. Chem. Soc.*, **40**, [9], 1361 – 1403, (1918).

18 Freundlich, H.: Of the adsorption of gases. Section II. Kinetics and energetics of gas adsorption, *Trans. Faraday Soc.*, 195 – 201, (1932).

19 Grigorio Jr., R., Capitao, R.C.: Morphology and phase transition of high melt temperature crystallized poly(vinylidene fluoride), *J. Mat. Sci.*, **35**, 299 – 306, (2000).

20 Salimi, A., Yousefi, A.A.: FTIR studies of β-phase crystal formation in stretched PVDF films, *Polym. Test.*, **22**, 699 – 704, (2003).

21 Broussely, M., Biensan, Ph., Bonhomme, F., Blanchard, Ph., Herreyre, S., Nechev, K., Staniewicz, R.J.: Main aging mechanisms in li ion batteries, *J. Power Sources*, **146**, 90 – 96, (2005).

22 Amine, K., Liu, J., Belharouak, I.: High-temperature storage and cycling of C-$LiFePO_4$/graphite Li-ion cells, *Electrochem. Comm.*, **7**, 669 – 673, (2005).

23 Wu, Y.P., Jiang, C., Wan, C., Holze, R.: Composite materials of silver and natural graphite as anode with low sensibility to humidity, *J. Power Sources*, **112**, 255 – 260, (2002).

24 Fu, L.J., Zhang, H.P., Wu, Y.P., Wu, H.Q., Holze, R.: Surface active Sites: an important factor affecting the sensitivity of carbon anode materials towards humidity, *Electrochem. Solid St.*, **8**, [9], A456 – A458, (2005).

25 Lee, H.-H., Wang, Y.-Y., Wan, C.-C., Yang, M.-H., Wu, H.-C., Shieh, D.-T.: A fast formation process for lithium batteries, *J. Power Sources*, **134**, 118 – 123, (2004).

26 Rasch, B., Cattaneo, E., Novak, P., Vielstich, W.: The influence of water on the oxidation of propylene carbonate on Platinum - an electrochemical, *in situ* FT-IT and On-Line MS Study, *Electrochimica Acta*, **36**, [9], 1397 – 1402, (1991).